ISBN: 978-3-95450-132-8 doi:10.18429/JACoW-IPAC2014-THPRO033

ELECTRON-BUNCH SHAPING FOR COHERENT INVERSE COMPTON SCATTERING

J. Thorne[1], P. Piot[1,2], I. Viti[1]
[1] Department of Physics, Northern Illinois Center for Accelerator & Detector Development, Northern Illinois University DeKalb, IL 60115, USA
[2] Accelerator Physics Center, Fermi National Accelerator Laboratory, Batavia, IL 60510, USA

Abstract

Producing high-quality X rays could have important applications to high-precision medical imaging and national security. Inverse Compton scattering involving the head-on collision of a relativistic electron bunch with a high-power laser offers a viable path toward the realization of a compact x-ray source. A method consisting in reflecting a short-pulse laser onto "relativistic mirror" (a moving thin sheet of electrons) has been proposed and recently demonstrated as a way to enhance the back-scattered photon flux by operating in the coherent regime. In this contribution we present preliminary particle-in-cell numerical simulations of the inverse Compton scattering process and especially investigate the impact of the electron-beam distributions that could substantially improve the x-ray production via coherent emission.

INTRODUCTION

The development of compact low-cost X-ray sources could have profound implications on a large number of applications including medicine, fundamental science, and security [1,2]. The availability of powerful off-the-shelve laser systems has sparked an outburst of compact X-ray-source concepts employing inverse Compton scattering (ICS). In this type of accelerator-based X-ray sources, an electron beam collides "head-on" with a high-intensity laser resulting in the production of radiation with upshifted frequency in the forward direction given by

$$\omega_x \simeq \frac{4\gamma^2\omega_L}{1+a_0^2/2+\gamma^2\theta^2}, \qquad (1)$$

where γ is the Lorentz factor associated to the electron beam, $\omega_L \equiv 2\pi c/\lambda_L$ (with λ_L being the laser wavelength), $\theta \ll 1$ is the observation angle with respect to the electron-beam's direction, and $a_0 \equiv eE/(k_L mc^2)$ is the laser normalized vector potential amplitude (here $k_L \equiv 2\pi/\lambda_L$ is the wave vector) . The on-axis single-electron angular-spectral fluence associated to the scattered radiation is [3]

$$\left(\frac{d^2U}{d\omega d\Omega}\right)_e \simeq \alpha a_0^2 N_L^2 \gamma^2, \qquad (2)$$

where α is the fine structure constant and N_L is the number of laser periods [3]. Therefore the efficiency of ICS is rather small and alternative solutions involve the production of coherently enhanced ICS radiation. In such a scheme, the electron beam is bunched at a scale comparable to the desired radiation wavelength so that in-phase emission of the scattered radiation occurs. When multi-particle coherence is significant, the expected on-axis angular-spectral fluence scales as [4]

$$\left(\frac{d^2U}{d\omega d\Omega}\right)_{tot} \simeq \left(\frac{d^2U}{d\omega d\Omega}\right)_e \left[N_e + N_e^2|F(\omega)|^2\right], \qquad (3)$$

where $F(\omega)$ is the Fourier transform of the line charge current distribution. Coherent enhancement can be achieved by either preparing an electron bunch with proper longitudinal distribution [5] or by forming a microbunched beam via a free-electron laser instability. In the latter case, the counter-propagating laser effectively acts as an optical undulator [6].

SIMULATION MODEL

In practice, when colliding an electron beam with a laser pulse an analytical prediction of the property of the scattered pulse is not possible and one usually relies on semi-analytical approach [7, 8]. Since our ultimate goal is to eventually develop a model that could also be used to explore the production of coherently-enhanced radiation, we focus on elaborating a model that works from first principles. Developing such a model is computationally challenging. First, the electron beam under consideration generally consists of a large number ($\sim 10^8$) of electrons. Second, the laser pulse cannot be modeled by a simple plane wave but needs to be described using a realistic field amplitude and transverse distribution. Therefore, to precisely understand the dynamics of the electrons in the laser-pulse fields, we rely on numerical simulations based on a finite-different time-domain (FDTD) technique combined with a particle-in-cell (PIC) approach. We implement the model within the WARP open-source framework available from Lawrence Berkeley National Laboratory [9]. WARP is capable of solving, from first principles, arbitrary electrodynamics problems [10].

The model especially takes advantage of WARP's capability to work in an arbitrary user-specified frame of reference [11, 12]. We therefore carry our simulation in the rest frame of the electron bunch. In this frame the laser collides with the stationary bunch and partially reflects off the bunch. In the electron-bunch frame the incident laser has a Lorentz-contracted wavelength $\lambda_L' = \lambda_L/[\gamma(1+\beta)]$ (where $\beta \equiv \sqrt{1-\gamma^{-2}}$). The fraction of the laser reflected off the bunch propagates backward in the rest frame and its wavelength is also λ_L'.

The WARP simulations are therefore performed in the Lorentz-boosted frame; see Fig. 1(a). Upon completion of

ISBN: 978-3-95450-132-8 doi:10.18429/JACoW-IPAC2014-THPRO033

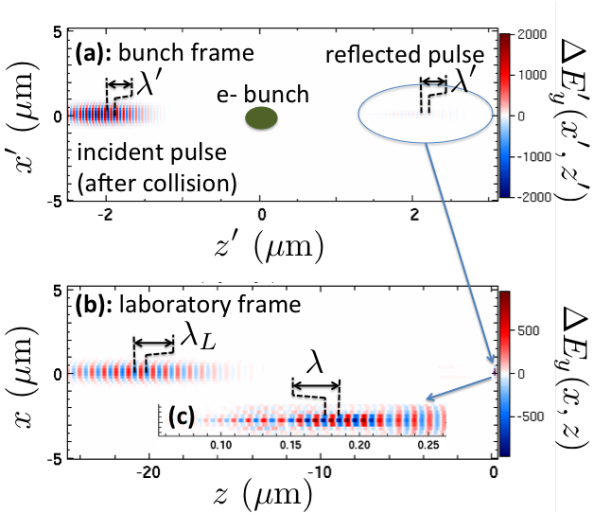

Figure 1: Example of "difference" electromagnetic fields computed in the reference frame (a) and Lorentz transformed in the laboratory frame (b). Inset (c) is a close up of the back-scattered pulse (frequency upshifted in the laboratory frame). The calculations were carried for $\gamma = 5$ and $a_0 = 0.1$ and the field snapshot is obtained a posteriori to the laser-electron collision.

the simulation the fields are Lorentz-transformed into the laboratory frame; see Fig. 1(b). In this Lorentz-transformation process the incident laser recovers its laboratory-frame wavelength λ_L while the backscattered laser has its wavelength further contracted in the laboratory frame to yield the final wavelength $\lambda = \lambda'/[\gamma(1+\beta)] = \lambda/[\gamma(1+\beta)]^2$, which recovers Eq. 1 in the limit of a relativistic electron ($\beta \simeq 1$), low laser intensity ($a_0 \ll 1$), and for on-axis observation angles ($\theta = 0$). Because of the weak field associated to the backscattered pulse, we carry our simulations in two steps. First, a vertically-polarized laser pulse launched from $z > 0$ is propagated along the $-\hat{z}$ direction and its field $\mathbf{E}_0(\mathbf{x}, t)$ recorded. In a second step, the electron bunch is introduced and the same laser pulse is propagated and the corresponding fields $\mathbf{E}(\mathbf{x}, t)$ are logged. The "difference" field defined $\Delta\mathbf{E}(\mathbf{x}, t) \equiv \{\mathbf{E} - \mathbf{E}_0\}(\mathbf{x}, t)$ is then computed; see Fig. 1. As observed in the latter figure, the difference-field map is non-vanishing at the present-time locations of the incident and reflected pulses [corresponding respectively to $z' \simeq \mp 2$ µm in Fig. 1(a)].

In our simulation the interaction occurs at $z' = 0$ (the location of the electron bunch center) and the electromagnetic fields associated to the back-scattered pulse are recorded on a spherical surface centered at $z' = 0$ with radius $R = 2$ µm, and with angular acceptance limited by the transverse sizes of the computation domains.These radiation fields, once transformed in the laboratory frame, are then Fourier transformed to yield the radiation's spectral properties. The simulations were validated for a few cases illustrated in Fig. 2: the obtained frequency agrees within a few percent with Eq. 1

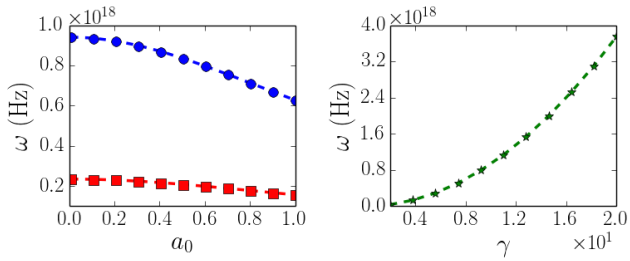

Figure 2: Benchmarking of WARP simulated radiation frequency (symbols) with analytical results from Eq. 1 as a function of the normalized vector potential (**left**) and electron bunch's Lorentz factor (**right**). In the left plot, the red and blue traces correspond respectively to $\gamma = 5$ and 20.

and the results reproduce the expected red-shift occurring as the value of a_0 is increased.

MULTI-PARTICLE COHERENCE

To explore the onset of multi particle coherence, we consider a vertically polarized laser with electric field $E_y(x, y, t) = E_0 \exp[-t^2/(2\sigma_t^2)] \exp[-r^2/(2\sigma_r^2)]$ where σ_t and σ_r are respectively the rms duration and transverse size ($r^2 \equiv x^2 + y^2$). The electron bunch it taken to be a cylin-

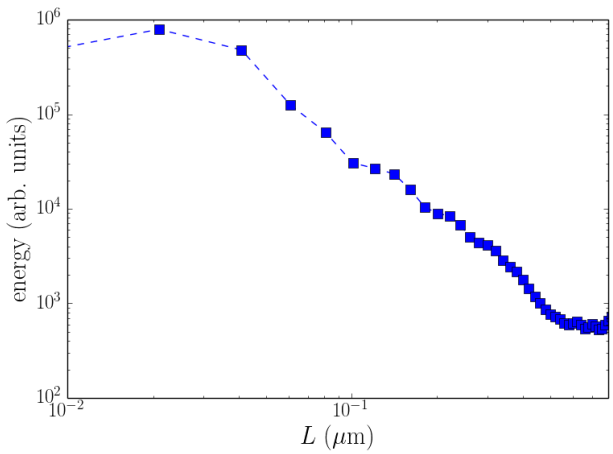

Figure 3: Simulated total energy deposited on the spherical "observation" surface as a function of electron-beam length L. The electron-beam radius is kept to $r = 1$ nm.

der with longitudinal size L and transverse radius ρ and is modeled as an ensembles of 5000 macroparticles. The laser parameters in the laboratory frame are set to $\lambda = 800$ nm, $\sigma_t = 10$ fs and $\sigma_r = 1$ µm. To investigate coherence effect we record the total energy $\propto |E|^2$ deposited on the observation surface using the electromagnetic fields Lorentz-transformed in the laboratory frame.

Given the shape of the electron bunch – a uniformly filled cylinder – we expect the longitudinal bunch form factor to be of the form $|F(\omega)|^2 = |1/(2\pi) \int_{-L/(2c)}^{+L/(2c)} dt e^{-i\omega t}|^2 \propto |\mathrm{sinc}(\frac{\omega L}{2c})|^2$ where $\mathrm{sinc}(x) \equiv \sin(x)/x$. Because of the nar-

ISBN: 978-3-95450-132-8 doi:10.18429/JACoW-IPAC2014-THPRO033

row bandwidth of ICS, the bunch form factor is essentially evaluated at $\omega = \omega_x$. Therefore as the electron-bunch length is scanned we expect the radiated power to display strong suppression for length satisfying $L = n\lambda$ where n is an integer. Figure 3 confirms this feature (small-oscillation features). Our simulations were limited to a very small computational domain to avoid prohibitive execution time and the bunch length in the rest frame was therefore limited to $L \leq 1$ μm. In addition the coherent enhancement observed 4×10^3 is consistent with the number of macro particle used to model the electron beam.

The influence of the transverse size is more intricate. First as the electron beam size is increased the number of electron participating in the ICS process might decrease due to partial transverse overlap between the electron and laser beams. Second, an increase is transverse size leads to a suppression of coherence and Eq. 3 needs to be altered to include a suppression factor [13] that depends on the transverse distribution. In our study we maintain the beam radius to a size below the laser-spot size so that we are dominated by the suppression factor. Figure 4 illustrate the simulated suppression of coherence as a function of the transverse size. The observed dependence is qualitatively similar to what presented in Ref. [13] for the case of undulator radiation.

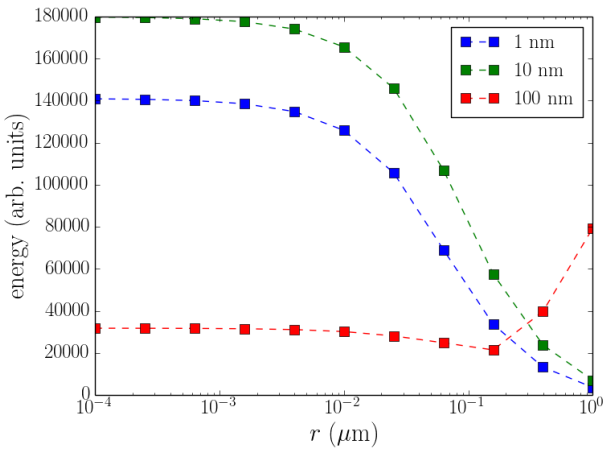

Figure 4: Simulated total energy deposited on the spherical "observation" surface as a function of electron-beam radius r. The three traces correspond to three cases of electron-beam length (shown in the legend). The laser parameters are given in the text and the condition $r \ll \sigma_r$ implies $r \leq 0.1$ μm.

CONCLUSION & OUTLOOK

We have developed a PIC FDTD model of the ICS interaction using the WARP framework. The model was successfully benchmarked against expected properties of ICS. It was finally used to explore coherently-enhanced ICS process for a simple case of a bunch with variable aspect ratio. The basic features of this coherently enhanced radiation were observed. The developed model will be expanded to explore more complex spatio-temporal shaping that could possibly enhance the efficiency of ICS sources.

ACKNOWLEDGMENTS

We are indebted to Dr. Jean-Luc Vay and Dr. David Grote from LBNL for making WARP available to us and for their valuable help with setting up and running the code. This work supported by the DARPA Axis program under contract N66001-11-1-4192 with MIT and by NIU's 2014 Undergraduate Special Opportunities in Artistry and Research (USOAR) Awards. PP is partially supported by DOE contract DE-AC02-07CH11359 to the Fermi research alliance LLC.

REFERENCES

[1] R.W. Schoenlein, et al., Science **274**, 236 (1996).

[2] H. N. Chapman, Nature. Mat. **8**, 299 (2009).

[3] S. Krinsky, IEEE Trans. Nuc. Sci. NS-30, 3078 (1983).

[4] J. S. Nodvick and D. S. Saxon, Phys. Rev. **96**, 180 (1954).

[5] W. S. Graves, et al., Phys. Rev. Lett. **108**, 263904 (2012).

[6] A.Bacci, et al., Phys. Rev. ST. AB. , **9**, 060704 (2006).

[7] E. S. Sarachik, et al., Phys. Rev. D **1**, 2738 (1970).

[8] E. Esarey, et al., Phys Rev E **48**, 3003 (1993).

[9] The WARP framework is available via GITHUB at `https://bitbucket.org/berkeleylab/warp`.

[10] J. L. Vay, D. P. Grote, R. H. Cohen, and A. Friedman, Comput. Sci. Disc. **5** 014019 (2012).

[11] J.-L. Vay, Phys. Rev. Lett 98, 130405 (2007); see also Phys. Rev. Focus **19**, 10 (2007).

[12] J.-L. Vay, et al., J. Comp. Phys. **230** (15), 5908 (2011).

[13] E. Saldin, et al., Nucl. Instrum. Methods Phys. Res., Sect. A 539, 499 (2005).